Pre-Steady-State Kinetic Study of Substrate Specificity of *Escherichia coli* Formamidopyrimidine−DNA Glycosylase†

Nikita A. Kuznetsov,‡ Vladimir V. Koval,‡ Dmitry O. Zharkov,‡ Yuri N. Vorobjev,‡ Georgy A. Nevinsky,‡ Kenneth T. Douglas,§ and Olga S. Fedorova*,‡

Institute of Chemical Biology and Fundamental Medicine, Siberian Branch of the Russian Academy of Sciences, and Novosibirsk State University, Novosibirsk 630090, Russia, and Wolfson Centre for Rational Design of Molecular Diagnostics, School of Pharmacy and Pharmaceutical Sciences, University of Manchester, Manchester M13 9PL, U.K.

Received April 23, 2006; Revised Manuscript Received September 22, 2006

ABSTRACT: Formamidopyrimidine−DNA glycosylase (Fpg) is responsible for removal of 8-oxoguanine (8-oxoG) and other oxidized purine lesions from DNA and can also excise some oxidatively modified pyrimidines [such as dihydrouracil (DHU)]. Fpg is also specific for a base opposite the lesion, efficiently excising 8-oxoG paired with C but not with A. We have applied stopped-flow kinetics using intrinsic tryptophan fluorescence of the enzyme and fluorescence of 2-aminopurine-labeled DNA to analyze the conformational dynamics of *Escherichia coli* Fpg during processing of good substrates (8-oxoG·C), poor substrates (8-oxoG·A), and substrates of unclear specificity (such as DHU and 8-oxoG opposite T or G). The analysis of fluorescence traces allows us to conclude that when the enzyme encounters its true substrate, 8-oxoG·C, the complex enters the productive catalytic reaction after ∼50 ms, partitioning the substrate away from the competing dissociation process, while poor substrates linger in the initial encounter complex for longer. Several intermediate ES complexes were attributed to different structures that exist along the reaction pathway. A likely sequence of events is that the damaged base is first destabilized by the enzyme binding and then everted from DNA, followed by insertion of several amino acid residues into DNA and isomerization of the enzyme into a pre-excision complex. We conclude that rejection of the incorrect substrates occurs mostly at the early stage of formation of the pre-eversion recognition complex, supporting the role of indirect readout in damage recognition.

Formamidopyrimidine−DNA glycosylase (Fpg) is a key enzyme involved in the repair of oxidatively damaged purines in bacterial DNA. A prototypical oxidative purine lesion, 8-oxo-7,8-dihydroguanine (8-oxoG, Figure 1), is premutagenic due to the ability of its deoxynucleoside (8-oxodG) to adopt a *syn* conformation and pair with dA in the Hoogstein mode (*1*−*3*). If adenine is inserted opposite 8-oxoG by a DNA polymerase, the next round of replication will lead to a G·C to T·A transversion in half of the progeny unless the 8-oxoG·A mispair is not restored to its original G·C form (*4*). Due to its mutagenicity and perhaps its structural effects in DNA, 8-oxoG and other oxidative lesions have been implicated in various pathologic conditions such as cancer and aging (*5*−*7*).

A three-tier enzymatic system ("GO system") has been evolved by most living organisms to deal with 8-oxoG and

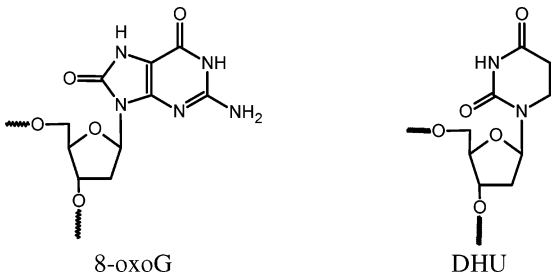

FIGURE 1: Structures of 8-oxoguanine (8-oxoG) and dihydrouracil (DHU).

the related lesions, 2,6-diamino-4-hydroxy-5-formamidopyrimidine (FapyG) (derived from guanine) and 4,5-diamino-5-formamidopyrimidine (FapyA) (derived from adenine), which are also miscoding and premutagenic (*8*, *9*). An 8-oxodG triphosphate hydrolase (MutT) prevents incorporation of 8-oxoG into DNA from the oxidized pool of dGTP, while a DNA glycosylase (Fpg) excises 8-oxoG paired with C, allowing the base excision repair machinery to replace 8-oxoG with a normal guanine base (*10*). Importantly, if Fpg can excise 8-oxoG from an 8-oxoG·A mispair, the product of adenine misinsertion, this excision would fix the G·C to T·A mutation. Thus, Fpg has low activity for this mispair (*10*, *11*), which is a preferred substrate for the third enzyme of the GO system, MutY DNA glycosylase (*12*−*14*). MutY removes adenine from 8-oxoG·A, initiating another attempt by DNA polymerase to insert a cytosine residue opposite

† This work was supported by grants from the Wellcome Trust (U.K.) (070244/Z/03/Z), the Presidium of the Russian Academy of Sciences (MCB Program, 10.5, 10.6), the Siberian Division of the Russian Academy of Sciences (Nos. 51, 60), RFBR (04-04-48171, 05-04-48619, 05-04-48322, 06-04-49263, 06-04-03034, 07-04-00191), the Russian Ministry of Education and Science (02.434.11.7064), and CRDF (Y1-B-08-08, Y1-B-08-16). N.A.K. and V.V.K. are supported by Young Scientist Fellowships from INTAS (05-109-4159, 04-83-3849).

* To whom correspondence should be addressed. Tel: +7 383 330 92 74. Fax: +7 383 333 36 77. E-mail: fedorova@niboch.nsc.ru.

‡ Institute of Chemical Biology and Fundamental Medicine and Novosibirsk State University.

§ University of Manchester.

10.1021/bi060787r CCC: $37.00
Published on Web 12/19/2006

8-oxoG. The resulting 8-oxoG·C pair is then a substrate for Fpg-dependent repair, as described above (*4*, *15*). The same system has been found operating in eukaryotes, most of which possess homologues of MutT and MutY, although the major eukaryotic 8-oxoG−DNA glycosylase (OGG1) is not a homologue of bacterial Fpg (*16*).

The preferential excision of 8-oxoG from 8-oxoG·C but not 8-oxoG·A by Fpg is crucial for the proper functioning of the GO system. As we have shown previously, Fpg effectively binds various dsODNs, including nonspecific ones (*17*−*19*). Steady-state kinetic studies (*11*, *20*) suggest that 8-oxoG·C is a 20−100-fold better substrate for Fpg than 8-oxoG·A, if the specificity constants ($k_{sp} = k_{cat}/K_M$) derived from the minimal Michaelis−Menten scheme are compared. Interestingly, 8-oxoG·G and 8-oxoG·T were reported to be even better substrates than 8-oxoG·C in terms of k_{sp} (*11*, *20*), although the exact reported values for all 8-oxoG-containing substrates vary considerably.

Another aspect of Fpg substrate specificity is its ability to excise lesions other than 8-oxoG from DNA. Fpg has been shown to excise more than 20 different lesions from synthetic dsODNs (reviewed in ref *21*) but only three (8-oxoG and formamidopyrimidine derivatives of A and G) from irradiated calf thymus DNA (*22*). In particular, dihydrouracil (DHU, Figure 1), a product of deamination of C and reduction of its 5,6 double bond, was shown to be a substrate when incorporated in ODNs but not to be excised from long DNA; this lesion is sometimes referred to as a "nonspecific substrate" for Fpg. The mechanisms of such discrimination may include competition from other lesions in long DNA or the relatively high concentration of the lesion in the experiments with oligonucleotides. The structure of *Bacillus stearothermophilus* Fpg complexed with DHU-containing DNA is available (*23*) and suggests that this lesion could be recognized in the enzyme's active site pocket in the same way as 8-oxoG but provides no clues to the relative efficiency of this lesion as a substrate for Fpg.

Structures of a number of complexes formed by Fpg proteins from different species (*23*−*29*) suggest that both the protein and the damaged DNA undergo extensive conformational changes in the course of DNA substrate binding and cleavage. Therefore, the reaction may proceed in several steps, and a simple Michaelis−Menten model may be insufficient for a correct kinetic analysis of Fpg substrate specificity. In addition, satisfying some criteria of Michaelis−Menten kinetics (e.g., a large excess of the substrate over the enzyme) is not always practical for DNA-dependent enzymes that often demonstrate substrate inhibition or product inhibition.

A stopped-flow approach allows extracting individual rate constants from the reactions that follow complex kinetic schemes, working in the pre-steady-state time range and under single-turnover conditions (*30*, *31*). As one of many examples, MutY DNA glycosylase is characterized by high affinity to its AP site product, and multiple-turnover kinetics can only reveal the rate of enzyme dissociation from the reaction product (*32*), while stopped-flow experiments resulted in the characterization of the complete kinetic scheme of the enzyme (*33*). We have recently applied stopped-flow pre-steady-state kinetics with intrinsic tryptophan fluorescence detection to investigate the fine detail of the conformational changes in the enzyme during the reactions catalyzed by *Escherichia coli* Fpg (*17*, *19*). It was found that recognition of 8-oxoG by Fpg involves at least five equilibrium steps leading to the final pre-excision complex. In principle, each of these steps could contribute to the functionally important discrimination between 8-oxoG·C and 8-oxoG·A or between 8-oxoG and DHU (*34*). In the present study, we have used stopped-flow kinetics with intrinsic Trp fluorescence detection to obtain detailed kinetic schemes for 8-oxoG opposite different bases and for DHU opposite C or G. In addition, we analyze DNA dynamics during the reaction by following fluorescence from a 2-aminopurine (2-aPu) label. Combining these two approaches, we have been able to describe the most likely sequence of events leading to preferential recognition of 8-oxoG·C and discrimination against other possible substrates by Fpg.

Table 1: Sequences of Oligodeoxynucleotides Used in This Work

shorthand	sequence[a]	X	Y
oG	d(CTCTCXCCTTCC)	8-oxoG	
DHU	d(CTCTCXCCTTCC)	DHU	
aPu-oG	d(CTCTYXCCTTCC)	8-oxoG	2-aPu
oG-aPu	d(CTCTCXYCTTCC)	8-oxoG	2-aPu
AP-aPu	d(CTCTCXYCTTCC)	AP	2-aPu
F-aPu	d(CTCTCXYCTTCC)	F	2-aPu
G-aPu	d(CTCTCGYCTTCC)		2-aPu
C	d(GGAAGGCGAGAG)		
A	d(GGAAGGAGAGAG)		
G	d(GGAAGGGGAGAG)		
T	d(GGAAGGTGAGAG)		
CCG	d(GGAAGCCGAGAG)		
GCC	d(GGAAGGCCAGAG)		

[a] Positions of modified nucleotides and their opposite-strand partners are underlined.

MATERIALS AND METHODS

Oligodeoxynucleotides and Enzymes. Fpg protein was purified as described (*19*). The fraction of the active enzyme (~90%) was determined by borohydride trapping. The reaction mixture included 2 μM enzyme, 25 mM potassium phosphate (pH 6.8), 100 mM NaCl, 100 mM $NaBH_4$, and varying amounts of oligonucleotide duplex containing an 8-oxoG residue positioned opposite C. The samples were incubated for 1 h at 25 °C, mixed with the loading buffer [50 mM Tris-HCl (pH 6.8), 2% SDS, 10% glycerol, 1% 2-mercaptoethanol, 0.1% bromophenol blue], and separated by 12% SDS−PAGE. The gel was stained with Coomassie and quantified using Gel-Pro Analyzer 4.0 software (Media Cybernetics, Silver Spring, MD).

The sequences of ODNs used in this work are listed in Table 1. ODNs were synthesized and purified as described (*17*, *19*) using phosphoramidites purchased from Glen Research (Sterling, VA). If needed, the modified strands were ^{32}P-labeled using [γ-^{32}P]ATP (Radioizotop, Moscow, Russia) and bacteriophage T4 polynucleotide kinase (New England Biolabs, Beverly, MA) according to the manufacturer's protocol. ODN duplexes were prepared by annealing modified and complementary strands taken at 1:1 molar ratio.

Stopped-Flow Studies. Stopped-flow measurements with fluorescence detection were carried out essentially as described (*17*, *19*) using a model SX.18MV stopped-flow spectrometer (Applied Photophysics, U.K.). To detect intrinsic Trp fluorescence only, $\lambda_{ex} = 290$ nm was used and

Scheme 1

$$E + S \leftrightarrow ES1 \leftrightarrow \cdots \leftrightarrow ESn \rightarrow EP1 \rightarrow \cdots EPm \leftrightarrow E + P$$

$\lambda_{em} > 320$ nm was followed as transmitted by a Schott filter WG 320 (Schott, Mainz, Germany). If 2-aPu was present in the ODNs, $\lambda_{ex} = 310$ nm was used to excite 2-aPu residues, and their emission was followed at $\lambda_{em} > 370$ nm (Corion filter LG-370); Trp fluorescence of the enzyme ($\lambda_{ex} = 290$ nm) was detected in this case using a Corion filter P10-340, which transmits a 10 nm wide band at ~340 nm to avoid overlapping with 2-aPu emission. When Trp fluorescence was studied, the enzyme concentration was 2 μM, and the substrate concentrations varied from 0.25 to 3 μM. To follow 2-aPu fluorescence, the substrate concentration was fixed at 2 μM, and the enzyme was varied from 0.25 to 3 μM. The kinetic data were obtained by numerical fitting using DynaFit software (BioKin, Pullman, WA) (*35*) as described (*17*, *19*). Each kinetic curve was averaged over at least three independent experiments after correction for internal absorption and bleaching (*17*, *19*). All kinetic schemes were built as sequences of *n* reversible and *m* irreversible steps and an enzyme−product complex equilibrium stage (see Scheme 1).

The conformity of the kinetic schemes with experimental data was assessed using a scree test. To do this, the dependence of standard deviations of the data residuals after fitting to an *n*-step binding model was plotted against *n*. A smooth decrease in the standard deviations leveled off after a certain number (*N*) of steps, indicating that the *N*-step kinetic scheme is indeed the minimal one (see Results). A similar analysis was done for the number of irreversible steps, *m*.

PAGE Time−Course Experiments. Reaction mixtures (20 μL) contained 50 mM Tris-HCl (pH 7.5), 50 mM KCl, 1 mM Na_2EDTA, 1 mM dithiothreitol, 9% glycerol, 1 μM ^{32}P-labeled substrate, and 2 μM enzyme. The reaction was initiated by adding the enzyme and allowed to proceed at 25 °C; aliquots (2 μL) were withdrawn as required and mixed with 3 μL of gel-loading dye containing 7 M urea. After PAGE, the gels were imaged by autoradiography and quantified by scanning densitometry using Gel-Pro Analyzer 4.0. Kinetic parameters were obtained by numerical fitting using OriginPro 7.5 software (OriginLab, Northampton, MA).

Molecular Dynamics of Fpg. The atomic structure of *E. coli* Fpg [PDB ID 1K82, chain A (*25*)] was taken for modeling. As this structure misses residues 217−224, their coordinates were restored using the following protocol. First, the initial structure of the backbone of the residues 217−224 has been taken from the corresponding residues 223−240 of the *B. stearothermophilus* Fpg [PDB ID 1R2Z (*23*)], chosen on the basis of a three-dimensional structure alignment of 1K82 and 1R2Z. Then, the side chains of residues 217−224 have been restored and their orientation optimized via the simulated annealing molecular dynamics protocol. A 2 ns molecular dynamics was then run using the Bison package (*36*). This program generates a classical molecular dynamics trajectory for a protein in water using the amber94 force field (*37*) and an analytical implicit solvent model (*38*). Use of a high-quality implicit solvent model allows a more effective sampling over the essential conformational space of a protein by excluding the dynamic friction inherent in the explicit solvent model.

RESULTS

Fpg Dynamics during Cleavage of Substrates with Different Bases Opposite the Lesion. The crucial property of Fpg as an antimutagenic enzyme is its ability do discriminate against 8-oxoG found in 8-oxoG·A mispairs (*10*, *11*); the opposite-base specificity in respect of G and T is less clear (see Discussion). We set out to investigate the kinetic models underlying this opposite-base preference. Fpg-catalyzed cleavage of dsODNs containing T, G, or A opposite 8-oxoG was followed in stopped-flow experiments with intrinsic Trp fluorescence detection. The results of these experiments are illustrated in Figure 2 (panel A). Rate constants for individual steps of the minimal reaction scheme (see Model Assessment below) were determined by global fitting and compared with our previous results for the 8-oxoG·C substrate (*17*, *19*). The respective fitted kinetic constants are listed in Table 2. (In all tables and the text, superscript indices "Trp" and "2-aPu" indicate the species deduced from or the values measured in or calculated from tryptophan fluorescence experiments and 2-aminopurine fluorescence experiments, respectively.)

It can be seen from Figure 2 (panels A) that the fluorescence time−course curves were qualitatively identical for all three substrates with different opposite bases. The fluorescence intensity dropped and rose starting at 2 ms to a ~10 s time point, with at least five discernible stages. At times >10 s the fluorescence increased steadily and then leveled; the plateau fluorescence decreased with increasing substrate concentration. The calculated reaction schemes for all three substrates with different opposite bases were identical to the scheme for binding and cleavage of 8-oxoG·C (*19*) and included five equilibrium binding steps, a single irreversible chemical step, and a product release equilibrium (Scheme 2). The comparison of fluorescence time−course curves for the mismatched substrates and for 8-oxoG·C (*19*) unequivocally indicates that the second phase (a modest increase in the fluorescence intensity) ensued much earlier for the "correct" substrate (8-oxoG·C) than for the mismatched ones.

We then compared the individual rate constants for all four Fpg substrates with different bases opposite the lesion. To facilitate comparison of general efficiency of Fpg working on different substrates, we have also calculated apparent macroscopic values (K_{bind}, K_M, k_{cat}, k_{sp}) for a reaction scheme with five binding equilibria using kinetic graph theory (see the footnote to Table 2 and Supporting Information). Overall, 8-oxoG·C was a much better substrate in comparison with the three mismatches (compare, for example, the values for K_{bind} or k_{sp} calculated for these substrates in Table 2). Interestingly, the most efficient step for opposite-base discrimination was the second equilibrium step (characterized by k_2 and k_{-2} rate constants, Scheme 2).

The equilibrium was shifted ~100-fold to the ES2 complex in 8-oxoG·C ($K_2 = 104$) but was approximately 1 for the other three substrates ($K_2 = 0.3-1.5$). On the other hand, two following steps of the reaction scheme were somewhat less efficient for 8-oxoG·C than for the mismatches ($K_3 = 0.15$ for 8-oxoG·C and 0.75−1.6 for the other opposite bases; $K_4 = 3.8$ for 8-oxoG·C and 3.0−11.4 for the other opposite bases). Rates of other microscopic steps in Scheme 1 were not significantly different between 8-oxoG·C and the three mismatches, so overall Fpg displayed an ~10-fold preference

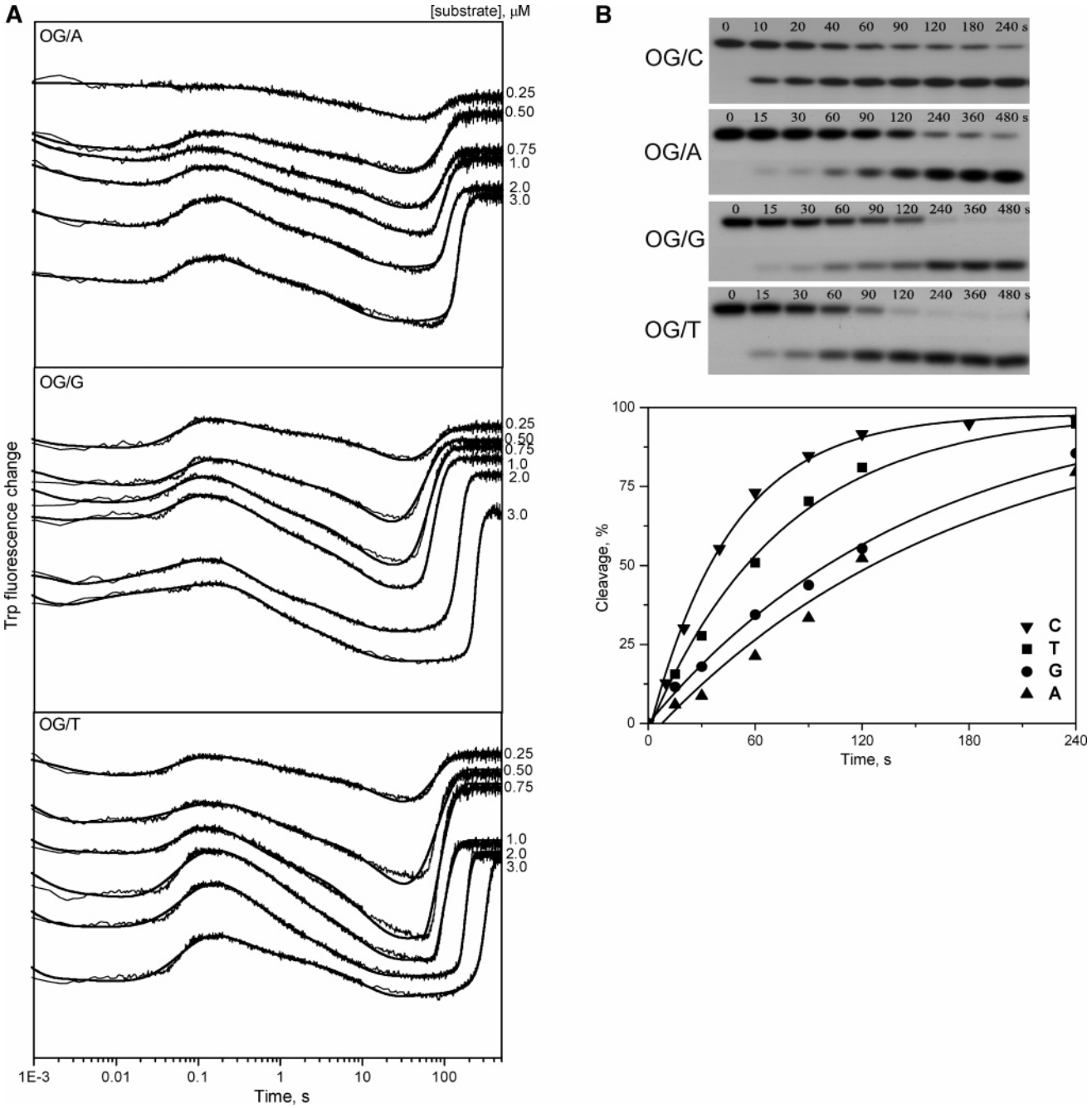

FIGURE 2: Processing of 8-oxoG·A, 8-oxoG·G, and 8-oxoG·T by Fpg. (A) Stopped-flow Trp fluorescence traces. Jagged traces represent experimental data; smooth curves are the results of fitting to a five-step kinetic model. Substrate concentrations are shown to the right of the plot; the enzyme concentration was 2 μM. (B) Time−course of product accumulation during cleavage of 8-oxoG·C, 8-oxoG·A, 8-oxoG·G, and 8-oxoG·T as revealed by PAGE.

for 8-oxoG·C at a macroscopic level. Thus, the stopped-flow studies indicate the following opposite-base preference of Fpg: C[dmt]T $\approx$ A $\approx$ G.

The opposite-base preference of Fpg was also confirmed by using PAGE to follow the substrate cleavage (Figure 2B). The respective time−course curves (Figure 2B) show that 8-oxoG·C is cleaved by Fpg much more efficiently than 8-oxoG·G and 8-oxoG·A, with 8-oxoG·T cleaved with an intermediate efficiency. Therefore, the opposite-base preference C > T > A $\approx$ G determined by PAGE is different from the stopped-flow results only for the 8oxoG·T mispair.

Model Assessment. In view of the multistage nature of the binding process and the importance of correct identification of the equilibria for their correlations with conformational changes in the protein, the model was statistically validated using the scree test (see Materials and Methods) to ensure that it indeed represents the minimal kinetic model adequately describing the results. Figure 3 illustrates the dependence of standard deviations of the data residuals after fitting to an *n*-step binding model on *n*, the number of steps in the model, for Fpg binding to 8-oxoG·C in a 1:1 molar ratio. It can be clearly seen that the smooth decrease in the standard deviations levels off after five steps, indicating that the five-step kinetic scheme is indeed the minimal one. The same result was obtained for all substrates investigated by intrinsic Trp fluorescence (data not shown). Thus, a kinetic scheme was considered minimal at *n* steps if at all experimentally investigated [Fpg]:[DNA] ratios the value of *n* fell into an

Table 2: Rate Constants of Conformational Transitions and Their Combinations in Fpg during Excision of 8-OxoG Opposite Different Bases

constant[a]	oG·C[b]	oG·T	oG·G	oG·A
k_1^{Trp}, $M^{-1}\,s^{-1}$	3.2×10^8	$(4.4 \pm 0.1) \times 10^8$	$(4.5 \pm 0.2) \times 10^8$	$(3.2 \pm 0.1) \times 10^8$
k_{-1}^{Trp}, s^{-1}	890	1240 ± 30	920 ± 20	870 ± 20
k_2^{Trp}, s^{-1}	250	24.3 ± 0.3	95.5 ± 2.2	92.7 ± 6.9
k_{-2}^{Trp}, s^{-1}	2.4	85.3 ± 1.4	119 ± 11	62.9 ± 5.3
k_3^{Trp}, s^{-1}	6.7	17.1 ± 0.2	9.6 ± 0.3	9.4 ± 0.3
k_{-3}^{Trp}, s^{-1}	46	10.4 ± 0.1	13 ± 0.7	12.5 ± 1.0
k_4^{Trp}, s^{-1}	9.1	10.9 ± 0.4	11.6 ± 0.3	6.9 ± 0.2
k_{-4}^{Trp}, s^{-1}	2.4	0.96 ± 0.03	1.30 ± 0.03	2.32 ± 0.08
k_5^{Trp}, s^{-1}	0.2	0.17 ± 0.01	0.24 ± 0.02	0.17 ± 0.01
k_{-5}^{Trp}, s^{-1}	0.03	0.020 ± 0.002	0.030 ± 0.002	0.015 ± 0.002
k_6^{Trp}, s^{-1}	0.04	0.026 ± 0.002	0.038 ± 0.002	0.031 ± 0.002
K_{EP}^{Trp}, M	2.0×10^{-6}	$(9.8 \pm 1.2) \times 10^{-6}$	$(8.7 \pm 0.3) \times 10^{-6}$	$(4.5 \pm 0.9) \times 10^{-6}$
K_{bind}^{Trp}, M^{-1}	202×10^6	18.7×10^6	24.4×10^6	16.3×10^6
K_M^{Trp}, M	8.7×10^{-9}	1.3×10^{-7}	9.2×10^{-8}	1.5×10^{-7}
k_{cat}^{Trp}, s^{-1}	0.019	0.019	0.026	0.020
k_{sp}^{Trp}, $M^{-1}\,s^{-1}$	2.2×10^6	1.5×10^5	2.9×10^5	1.3×10^5

[a] $K_{bind} = \sum_{i=1}^{i=5}\prod_{j=1}^{j=i} K_j$ for five-step binding (Scheme 2). K_M and k_{cat} values were calculated from the equations derived for Scheme 2 using enzyme kinetic graph theory (*56*), as shown in the Supporting Information. $k_{sp} = k_{cat}/K_M$. Estimated value ± standard error of the estimate is shown. [b] From ref *19*; cf. the values reported in Table 4 for 8-oxoG·C with 2-aPu substitutions.

Scheme 2

$$E + S \underset{k_{-1}^{Trp}}{\overset{k_1^{Trp}}{\rightleftharpoons}} ES1^{Trp} \underset{k_{-2}^{Trp}}{\overset{k_2^{Trp}}{\rightleftharpoons}} ES2^{Trp} \underset{k_{-3}^{Trp}}{\overset{k_3^{Trp}}{\rightleftharpoons}} ES3^{Trp} \underset{k_{-4}^{Trp}}{\overset{k_4^{Trp}}{\rightleftharpoons}}$$

$$ES4^{Trp} \underset{k_{-5}^{Trp}}{\overset{k_5^{Trp}}{\rightleftharpoons}} ES5^{Trp} \xrightarrow{k_6^{Trp}} EP \overset{K_{EP}^{Trp}}{\rightleftharpoons} E + P$$

early scree region (an apparent breakpoint in Figure 3) of the plot rather than into the steep descent region.

Fpg Dynamics during Cleavage of Dihydrouracil. DHU has been described as a nonspecific substrate for Fpg, since it is inefficiently excised by this enzyme from long DNA targets (*22*) but is an excellent substrate in ODNs (see ref *20* and discussion therein). It has been suggested that recognition of 8-oxoG and DHU by Fpg could involve different conformational changes in the protein molecule (*20*). Thus, we have used substrates containing DHU opposite C (a mismatch previously investigated by steady-state kinetics) or G (the context in which DHU would naturally arise in the cell by reductive deamination of C) to determine the kinetic scheme and rate constants of Fpg action on such lesions. The results of stopped-flow experiments with intrinsic Trp fluorescence detection are shown in Figure 4 and Table 3. In the case of DHU, Scheme 2 with five binding equilibria was also valid. Processing of the substrates was clearly observed; however, it was less efficient overall than

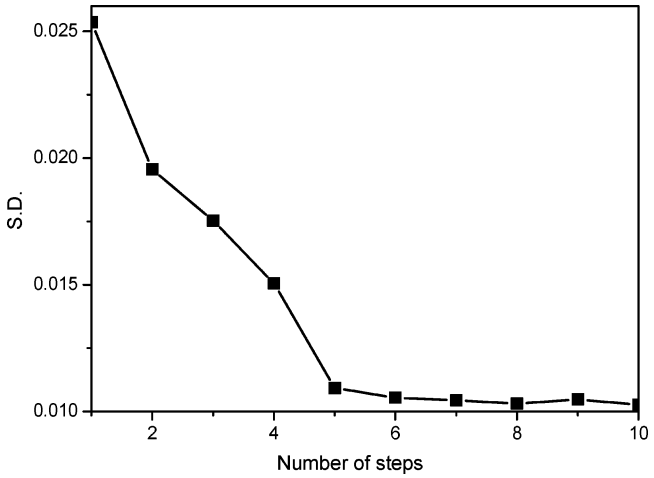

FIGURE 3: Scree test for Fpg reaction schemes. Fpg and ODN were taken in a 1:1 molar ratio. Standard deviation (SD) of the residuals after fitting to an *n*-step binding model is plotted against *n*. The number of steps corresponding to the beginning of the shallow-slope (scree) region is considered minimal for adequately describing the binding.

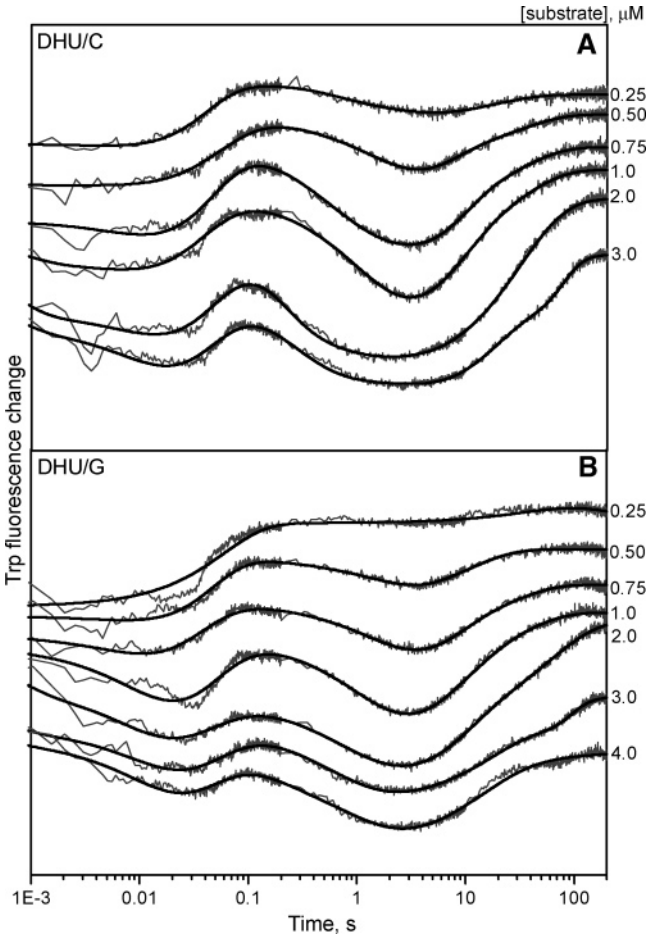

FIGURE 4: Processing of DHU·C and DHU·G by Fpg. (A) Stopped-flow Trp fluorescence traces for DHU·C. Jagged traces represent experimental data; smooth curves are the results of fitting to a five-step kinetic model. Substrate concentrations are shown to the right of the plot; the enzyme concentration was 2 μM. (B) Same as (A) but for DHU·G.

Table 3: Rate Constants of Conformational Transitions and Their Combinations in Fpg during Excision of DHU Opposite C or G

constant[a]	DHU·G	DHU·C
k_1^{Trp}, M^{-1} s^{-1}	$(240 \pm 4) \times 10^6$	$(234 \pm 4) \times 10^6$
k_{-1}^{Trp}, s^{-1}	1130 ± 20	1270 ± 20
k_2^{Trp}, s^{-1}	59.2 ± 3.3	46.5 ± 1.1
k_{-2}^{Trp}, s^{-1}	174 ± 9	136 ± 5
k_3^{Trp}, s^{-1}	48.4 ± 11.8	35.7 ± 2.7
k_{-3}^{Trp}, s^{-1}	7.7 ± 0.7	9.2 ± 0.4
k_4^{Trp}, s^{-1}	4.7 ± 0.7	8.9 ± 0.5
k_{-4}^{Trp}, s^{-1}	0.15 ± 0.02	0.58 ± 0.06
k_5^{Trp}, s^{-1}	0.11 ± 0.01	0.16 ± 0.02
k_{-5}^{Trp}, s^{-1}	0.033 ± 0.005	0.11 ± 0.02
k_6^{Trp}, s^{-1}	0.025 ± 0.005	0.078 ± 0.007
K_{EP}^{Trp}, M	$(9.8 \pm 1.2) \times 10^{-6}$	$(2.5 \pm 0.3) \times 10^{-6}$
K_{bind}^{Trp}, M^{-1}	6.3×10^7	9.7×10^6
K_M^{Trp}, M	3.7×10^{-8}	1.6×10^{-7}
k_{cat}^{Trp}, s^{-1}	0.016	0.033
k_{sp}^{Trp}, M^{-1} s^{-1}	4.3×10^5	2.0×10^5

[a] See footnote to Table 2 for definitions of K_{bind}, K_M, k_{cat}, and k_{sp}. Estimated value ± standard error of the estimate is shown.

for 8-oxoG·C, on a par with 8-oxoG opposite other bases (cf. K_{bind} and k_{sp} in Tables 2 and 3). DHU was excised somewhat better (~2.2-fold if k_{sp} are compared) when placed opposite G than when put opposite C, mostly due to a more efficient channeling through the last three equilibria; however, k_6 (and k_{cat}) values were greater for DHU·C, presumably reflecting better stabilization of the Michaelis complex (or the transition state) due to a more efficient interaction of the critical Arg-108 residue with the C base (see Discussion). Interestingly, the reaction kinetics were also similar to those for 8-oxoG opposite A, G, or T, with low K_2 and high K_3 and K_4 values, supporting the idea that the recognition of DHU by Fpg follows a different kinetic scheme than does recognition of 8-oxoG, which could reflect a fundamental difference in conformational rearrangements during these two processes (see Discussion below and in ref *20*).

DNA Dynamics during Binding to Fpg. Intrinsic Trp fluorescence only allows one to follow the protein movements during DNA binding. In order to analyze the DNA dynamics in this process and to relate these with the protein dynamics, we introduced 2-aPu deoxynucleotides either 5′ or 3′ next to the lesion (substrates designated aPu-oG and oG-aPu, respectively). The intensity of emission of 2-aPu is strongly influenced by its environment; in particular, it is partially quenched when 2-aPu is stacked in a DNA duplex (*39*). Since the stacking is partially disrupted in the three-dimensional structure of Fpg (*25*), we reasoned that changes in 2-aPu fluorescence could provide a good way to observe events associated with the lesion eversion.

Reactions of Fpg with the 2-aPu-containing duplexes (oG-aPu)·(CCG) and (aPu-oG)·(GCC) were investigated following either the intrinsic Trp fluorescence of Fpg or fluorescence of the 2-aPu residues. As the sequence of the substrates was changed by introduction of 2-aPu, we have initially investigated the effect of the 2-aPu residue and its position relative to 8-oxoG on the kinetics determined from the intrinsic Trp fluorescence of Fpg (Figure 5). Although the fluorescence intensities changed somewhat with the 2-aPu-containing substrates, the five-step binding scheme (Scheme 2) was again revealed by Trp fluorescence experiments (Table 4). Figure 6 shows time courses of 2-aPu fluorescence in the duplexes containing 2-aPu residues 5′ or 3′ to 8-oxoG,

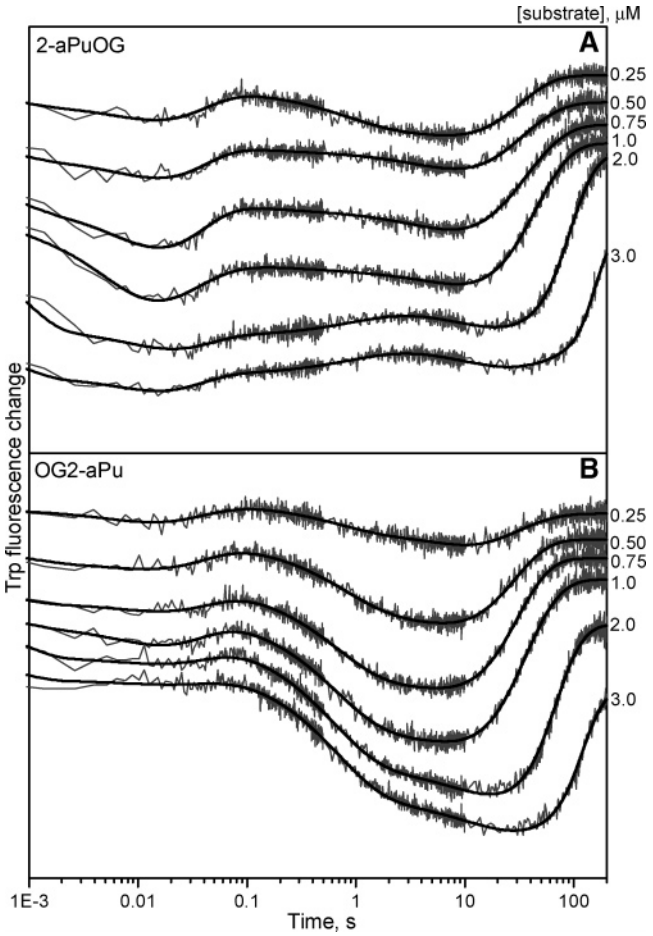

FIGURE 5: Stopped-flow Trp fluorescence traces for substrates (aPu-oG)·(CCG) and (oG-aPu)·(GCC). Jagged traces represent experimental data; smooth curves are the results of fitting to a five-step kinetic model. Substrate concentrations are shown to the right of the plot; the enzyme concentration was 2 μM.

Table 4: Rate Constants of Conformational Transitions and Their Combinations in Fpg during Excision of 8-OxoG Adjacent to 2-aPu from 8-oxoG·C Mispairs

constant[a]	(oG-aPu)·(CCG)	(aPu-oG)·(GCC)
k_1^{Trp}, M^{-1} s^{-1}	$(350 \pm 70) \times 10^6$	$(689 \pm 6) \times 10^6$
k_{-1}^{Trp}, s^{-1}	900 ± 180	847 ± 16
k_2^{Trp}, s^{-1}	245 ± 9	743 ± 19
k_{-2}^{Trp}, s^{-1}	11.6 ± 0.2	44.2 ± 1.9
k_3^{Trp}, s^{-1}	3.56 ± 0.03	3.3 ± 0.2
k_{-3}^{Trp}, s^{-1}	39.1 ± 0.05	60.9 ± 2.7
k_4^{Trp}, s^{-1}	14.3 ± 0.05	12.2 ± 0.2
k_{-4}^{Trp}, s^{-1}	1.21 ± 0.01	3.00 ± 0.08
k_5^{Trp}, s^{-1}	0.131 ± 0.008	0.20 ± 0.02
k_{-5}^{Trp}, s^{-1}	0.004 ± 0.0006	0.003 ± 0.0002
k_6^{Trp}, s^{-1}	0.034 ± 0.001	0.029 ± 0.0004
K_{EP}^{Trp}, M	$(2.26 \pm 0.01) \times 10^{-6}$	$(3.4 \pm 0.1) \times 10^{-6}$
K_{bind}^{Trp}, M^{-1}	286×10^6	220×10^6

[a] See footnote to Table 2 for a definition of K_{bind}. Estimated value ± standard error of the estimate is shown.

natural abasic site (AP), tetrahydrofuran abasic site (F), or undamaged G. For the undamaged G substrate, the fluorescence intensity increased slightly at times <10 ms (Figure 6) due to a shift of 2-aPu to a more hydrophilic environment, possibly indicating destabilization of the DNA double helix upon binding the enzyme. No such increase was observed for the F-containing substrate (Figure 6), since the lack of a base next to 2-aPu prevented quenching of 2-aPu fluores-

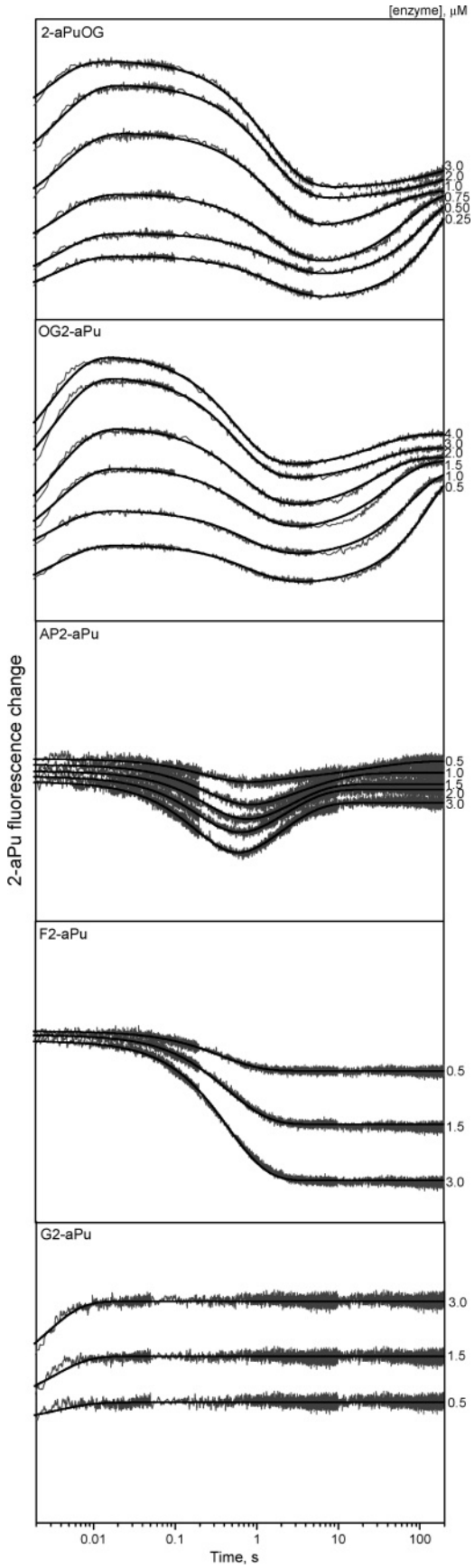

FIGURE 6: Stopped-flow 2-aPu fluorescence traces for (aPu-oG)·(CCG), (oG-aPu)·(GCC), (AP-aPu)·(GCC), (F-aPu)·(GCC), and (G-aPu)·(GCC). Jagged traces represent experimental data; smooth curves are the results of fitting to a kinetic scheme (Scheme 3). Enzyme concentrations are shown to the right of the plot; the substrate concentration was 2 μM.

Scheme 3

$$E + S \underset{k_{-1}^{2\text{-aPu}}}{\overset{k_1^{2\text{-aPu}}}{\rightleftharpoons}} ES1^{2\text{-aPu}} \underset{k_{-2}^{2\text{-aPu}}}{\overset{k_2^{2\text{-aPu}}}{\rightleftharpoons}} ES2^{2\text{-aPu}} \xrightarrow{k_3^{2\text{-aPu}}} EP \overset{K_{EP}^{2\text{-aPu}}}{\rightleftharpoons} E + P$$

cence in the first place. The drop in 2-aPu fluorescence intensity was observed at times <1 s. The AP-containing substrate (Figure 6) also showed no initial (<10 ms) increase in fluorescence but demonstrated a decrease at 0.1−1 s and then an increase at 1−10 s. Both 8-oxoG-containing substrates, (oG-aPu)·(CCG) and (aPu-oG)·(GCC), displayed a more complicated time course (Figure 6), with an increase in the fluorescence intensity at <10 ms, a drop at 0.1−1 s, and another increase at 1−10 s.

Only two binding equilibria were sufficient to describe conformational changes in DNA in minimal terms (Scheme 3). Table 5 lists the values of the rate constants determined for this scheme. There was little difference in the 2-aPu fluorescence curves generated during processing of substrates containing the fluorescent base 5′ or 3′ to the lesion, despite the different nature of amino acids contacting these bases in the Michaelis complex of Fpg [e.g., the 5′-base is stacked against the guanidinium group of Arg-108, whereas the 3′-base contacts the side chains of Met-73 and, to a lesser degree, of Phe-110 (*25*)]. Comparison of the macroscopic parameters calculated for either type of experiment (e.g., K_{bind} in Tables 2 and 4) also reveals little difference between 8-oxoG·C-containing substrates with or without 2-aPu, indicating that this fluorescent label does not interfere with productive binding and cleavage of damaged DNA by Fpg. Thus, these fluorescence experiments with 2-aPu reflect the true dynamics of DNA binding to Fpg.

To analyze the relationship between different species in Schemes 2 and 3, we performed a kinetic simulation of both reaction pathways using the rate constants determined by Trp fluorescence and 2-aPu fluorescence for the same substrate and compared the time courses of appearance and disappearance of the kinetic species. Figure 7 illustrates the results obtained for the (aPu-oG)·(GCC) substrate, which suggest that $ES1^{2-aPu}$ likely corresponds to $ES2^{Trp}$ and $ES3^{Trp}$ and $ES2^{2-aPu}$ likely corresponds to $ES4^{Trp}$ and $ES5^{Trp}$. Similar results were obtained for the (oG-aPu)·(CCG) substrate.

Modeling of Fpg Dynamics. The conformational dynamics of the free Fpg has been investigated over a 2 ns equilibrium molecular dynamic trajectory. Fluctuations in the total molecular surface area over the equilibrium trajectory are shown in Figure 8A. It can be seen that the molecular surface fluctuations can reach ~200 Å^2 at a fast picosecond scale and average ~100 Å^2 at a 100 ps scale, and the surface area is stable over a nanosecond scale. This behavior allows us to assume that we observed the equilibrium thermal fluctua-

Table 5: Rate Constants of Conformational Transitions in DNA during Excision of 8-OxoG from 8-OxoG·C Mispairs by Fpg

constant	(oG-aPu)·(CCG)[a]	(aPu-oG)·(GCC)
k_1^{2-aPu}, M^{-1} s^{-1}	(93.1 ± 0.4) × 10^6	(75.0 ± 1.1) × 10^6
k_{-1}^{2-aPu}, s^{-1}	143 ± 2	146 ± 5
k_2^{2-aPu}, s^{-1}	1.26 ± 0.08	0.67 ± 0.01
k_{-2}^{2-aPu}, s^{-1}	0.8 ± 0.0002	0.32 ± 0.01
k_3^{2-aPu}, s^{-1}	0.052 ± 0.002	0.033 ± 0.002
K_{EP}^{2-aPu}, M	(1.6 ± 0.3) × 10^{-6}	(1.19 ± 0.02) × 10^{-6}

[a] Estimated value ± standard error of the estimate is shown.

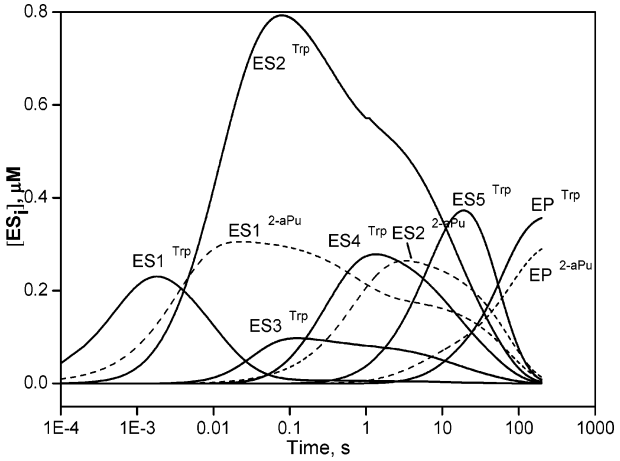

FIGURE 7: Kinetic simulation of the time−course of appearance and disappearance of different intermediates evident from intrinsic Trp fluorescence and 2-aPu fluorescence: solid line, intrinsic Trp fluorescence; dashed line, 2-aPu fluorescence. The intermediates are labeled according to Schemes 1 and 3, respectively. The simulations were run at [E]0 = [S]0 = 1 μM; see Materials and Methods for other details. The most probable attribution of different intermediates follows. Intermediates detected by Trp fluorescence: ES1^{Trp}, Fpg bound to DNA nonspecifically; ES2^{Trp}, pre-eversion recognition complex; ES3^{Trp}, the complex with the damaged nucleoside bound in the enzyme's active site; ES4^{Trp}, the complex with the damaged nucleoside bound in the enzyme's active site and the void-filling residues plugged into the DNA helix; ES5^{Trp}, final Michaelis complex; EP^{Trp}, enzyme−product complex. Intermediates detected by 2-aPu fluorescence: ES1^{2-aPu}, complex with 2-aPu unstacked from the adjacent 8-oxoG by DNA destabilization or 8-oxodG eversion; ES2^{2-aPu}, complex with 2-aPu stacked against the void-filling enzyme residues; EP^{2-aPu}, enzyme−product complex.

tions of the Fpg molecular structure. Four snapshots of the molecular structure of the Fpg taken with the 500 ps step are shown in Figure 8B. It can be seen that the Fpg maintains the overall shape of the DNA binding cleft. The distribution of the conformational mobility of the residue over the sequence is shown in Figure 8C. It can be seen that there are three segments of the sequence with the mobility of the residues sharply increased (residues 30−40, 100−110, and 250−260) by a factor of 3−4 over the baseline. The first highly mobile segment includes the Trp-34 residue which moves with a ~12 Å amplitude (Figure 8C). The principal component analysis of the essential conformational movements (*40*) shows that the main mode of the conformational movement is a flip-flop move of two domains of Fpg which form the DNA binding cleft (see the Supporting Information movie).

DISCUSSION

Kinetic Model Attribution. The structure of Fpg bound to the lesion, obtained by us and by other groups (*23*, *25*−*28*), reveals that the damaged nucleoside is everted from DNA and resides in the enzyme's deep active site pocket. DNA is severely kinked at the point of the lesion, and several protein residues (Met-73, Arg-108, and Phe-110 in *E. coli* Fpg) are inserted in the DNA double helix to fill the void created by eversion of the damaged nucleoside, partially mimicking the base stacking through $\pi-\pi$ or van der Waals interactions with the aromatic or hydrophobic protein moieties. Such extensive rearrangement of protein and DNA molecules is unlikely to be achieved in a single binding step, making the

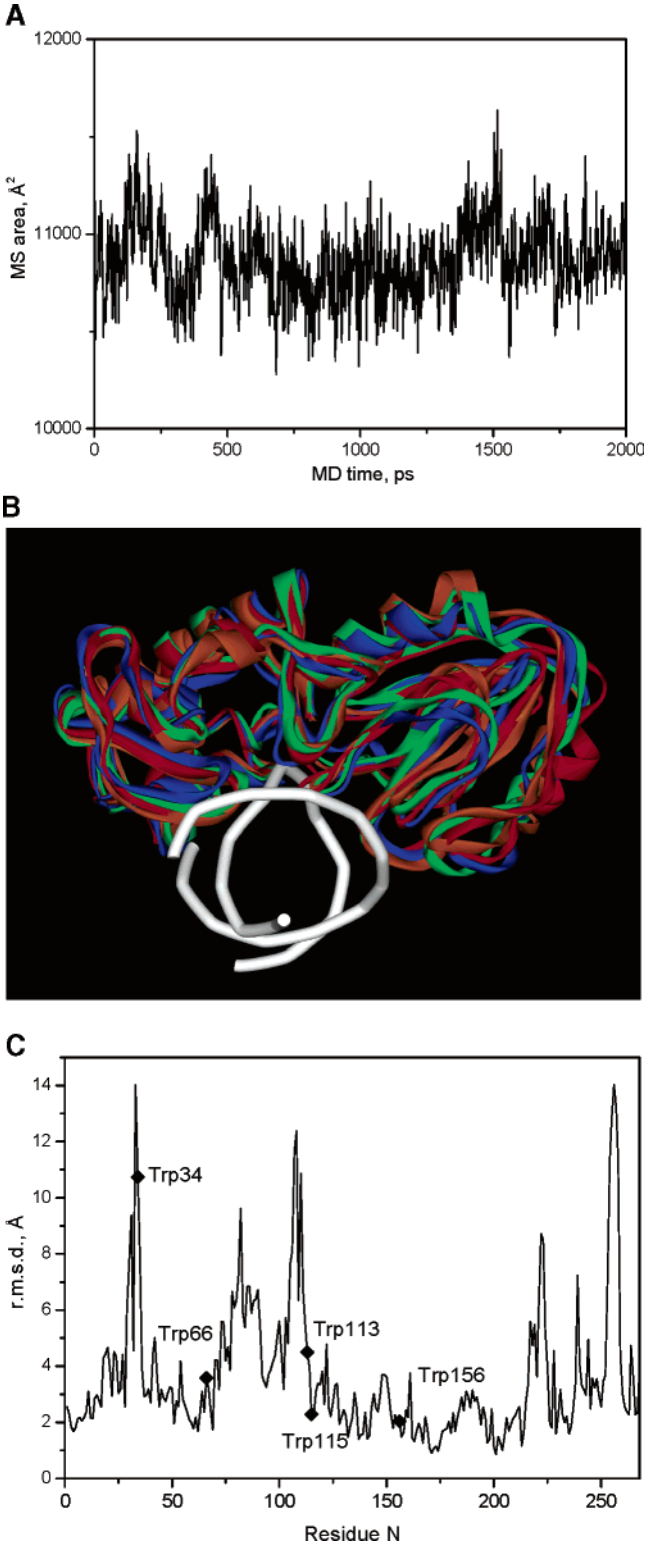

FIGURE 8: Molecular dynamics of Fpg. (A) Molecular surface of Fpg over the equilibrium molecular dynamic trajectory. (B) Four snapshots of the Fpg protein structure (red, 500 ps; orange, 1000 ps; green, 1500 ps; blue, 2000 ps). (C) Average rmsd per residue calculated over the whole 2 ns molecular dynamic trajectory. Diamonds indicate the positions of the Trp residues in the Fpg sequence.

multistep binding model structurally justified. In our previous work (*19*) we have combined stopped-flow data and structural information available for Fpg to attribute five equilibrium steps in Fpg-mediated processing of 8-oxoG·C to the most likely conformational changes in the protein molecule.

These equilibria (Scheme 2) were suggested to correspond respectively to (i) nonspecific binding of Fpg to the lesion and formation of ES1, (ii) formation of the pre-eversion recognition complex ES2, (iii) eversion of the damaged nucleoside from DNA into the enzyme's active site pocket and formation of ES3, (iv) insertion of the enzyme residues into DNA to fill the void in the helix ("plugging") and formation of ES4, and (v) isomerization of the enzyme globule to the final pre-excision complex and formation of ES5. The last step was suggested to involve conformational changes in the flexible enzyme loop that forms a large part of the base-binding pocket (*41*, *42*).

In the present study, we have extended the pre-steady-state kinetic analysis into a range of other Fpg substrates and supplemented it with the analysis of 2-aPu fluorescence in the stopped-flow mode. The five-step binding kinetics revealed by the enzyme's internal tryptophan fluorescence for 8-oxoG·C held true for all substrates we have studied. The analysis of 2-aPu fluorescence provided additional insight into the nature of different steps in the binding model. Five reversible steps in Scheme 2 correspond to only two fluorescently discernible steps in Scheme 3. In the course of binding of the enzyme to DNA containing a damaged nucleoside flanked by a 2-aPu residue, the fluorescence of the latter can be changed by DNA kinking, by eversion of the damaged nucleoside, and by plugging of the void by the protein residues. The characteristic times of appearance and disappearance of different ES intermediates suggest that the first detectable changes in 2-aPu fluorescence ($\leq$10 ms, Figure 6) occur after the formation of the $ES1^{Trp}$ recognition complex (Scheme 2) but likely before the eversion of 8-oxodG. Hence, the stage that was attributed to the $ES2^{Trp}$ complex formation (*19*) coincides with the stage of DNA destabilization, indicating that the recognition might be initiated by a perturbation of the canonical structure in the vicinity of the lesion. The exact nature of this perturbation cannot be established at present; the possibilities include DNA kinking, "pinching" of the adjacent phosphates to introduce strain into DNA, or initial stages of the eversion. The role of DNA destabilization in recognition by Fpg has been extensively discussed in the literature (see below), and our data seem to add weight to this hypothesis.

The next step that can be discerned by 2-aPu fluorescence (Figure 6, time $\sim$1 s) coincides with the formation of the $ES4^{Trp}$ complex. In our previous work this stage of the tryptophan fluorescence curve was attributed to plugging (*19*). The new experiments support this attribution further, since the fluorescence intensity of 2-aPu most probably changes when three residues of Fpg are inserted into DNA and alter the environment of the fluorescent base. The previous stage, the formation of the $ES3^{Trp}$ complex, can then be attributed to the eversion of 8-oxoG. A "pinch−pull−push" mode of action was proposed by Wong et al. for *E. coli* uracil−DNA glycosylase based on stopped-flow data (*43*). On the basis of our attribution, we advocate a similar model for Fpg, with a note that since the insertion of the void-filling residues does not actively "push" the damaged base from the helix, the model should be more correctly termed "pinch−pull−plug", in accordance with the scheme proposed by Stivers and colleagues (*44*−*46*).

A rival "pinch−push−pull" model of DNA glycosylase action involves the inserted groups of the enzyme actively pushing the damaged base to initiate the eversion. This model has been contemplated for human uracil−DNA glycosylase and human 8-oxoguanine−DNA glycosylase OGG1 (structurally unrelated to Fpg) based purely on structural data (*47*, *48*) but so far has not been probed kinetically. This scheme seems less likely in the case of Fpg, as it would require the time course of appearance of the $ES2^{2-aPu}$ complex to coincide with $ES3^{Trp}$ and $ES4^{Trp}$ (see Figure 7 for the complex attribution), with the latter two also likely coalescing into a single step as plugging and the eversion must proceed simultaneously in this scheme; neither of these predictions agrees with our observations.

To estimate the possible contribution of different Trp residues in the Fpg fluorescence, we have modeled the dynamics of the Fpg molecule. Although no set of *E. coli* Fpg structures is available to approximate the movement of the Fpg−DNA along the reaction coordinate, we have addressed the question, what parts of the enzyme are the most mobile in a single structure, that of Fpg covalently complexed with DNA in a reduced Schiff base intermediate (*25*). Fluorescence of Trp residues in such regions is likely to be most responsive to the conformational movements of the enzyme molecule. Consistently with our earlier suggestion (*19*), Trp-34 demonstrated the highest rmsd in a 2 ns molecular dynamics, falling into one of the most flexible regions of the Fpg molecule (Figure 8C). Trp-156, another possible candidate for a residue whose fluorescence might change during the reaction course, was in fact the least mobile of all Trp residues (Figure 8C). However, its contribution to the fluorescence changes at the earlier stages of the reaction cannot be excluded, especially if Fpg undergoes gross structural changes upon DNA binding, as was shown for endonuclease VIII, an enzyme closely related to Fpg (*49*).

Opposite-Base Specificity of Fpg. Except for the well-reproducible fact that Fpg prefers 8-oxoG·C as a substrate over 8-oxoG·A, the opposite-base specificity of this enzyme is still an open question. It was earlier reported (with no kinetics provided) that Fpg cleaves the substrates with the order of opposite-base preference C $\geq$ T $\gg$ G $\gg$ A (*50*) or C $\approx$ T $\approx$ G $\gg$ A (*51*). On the other hand, in steady-state Michaelis−Menten kinetic experiments Fpg was found to prefer 8-oxoG·G and 8-oxoG·T over 8-oxoG·C (*10*, *11*, *20*), with the specificity constant ($k_{sp} = k_{cat}/K_M$) being $\sim$5−30-fold higher for the first two mispairs. Since Fpg flips the damaged base out of the double helix to gain access to C1′, the target of the nucleophilic attack in the course of the reaction, this preference for 8-oxoG·G and 8-oxoG·T has been rationalized in terms of destabilization of dsDNA at the site of the lesion (*11*, *52*). Although these events also may be considered premutagenic, neither 8-oxoG·G nor 8-oxoG·T would be normally found in DNA, and thus little evolutionary pressure has been probably placed on Fpg to avoid excision of 8-oxoG from these mispairs. Structures of Fpg from *B. stearothermophilus* covalently complexed with the DNA reaction product containing estranged C, G, or T indicate that C is optimally contacted by an absolutely conserved arginine residue in the enzyme, with G and T allowed but less optimal (*27*). No structural information on the estranged A is available. In general, the exact mechanism of the opposite-base discrimination by Fpg is still unclear.

Here we have studied the opposite-base specificity of Fpg by fast kinetics and obtained the following order of opposite-base preference: C ≫ T ≈ G ≈ A. The sequence of the 12-mer duplex substrate used in our studies was identical to a central part of the 23-mer duplex substrates for which the steady-state kinetics was reported (*11*, *20*). The steady-state kinetic data available in the literature show a significant variance even with the same substrate, with k_{cat} values disagreeing 1.5−3-fold, K_M values, 8.6−57-fold, and k_{cat}/K_M ratios, 5.7−33-fold. Such disagreement may be explained by excess concentrations of Fpg used in the earlier studies (*11*) that could shift the reaction conditions into a range unsuitable for the Michaelis−Menten scheme and by possible differences in the substrate range and time point at which the initial rate has been determined. On the other hand, stopped-flow kinetics is usually done under single-turnover conditions and high enzyme and substrate concentrations, allowing one to avoid the problems arising when extracting K_M and k_{cat} constants for complex reaction schemes.

To confirm the order of the opposite-base preference obtained in the stopped-flow experiments with fluorescence detection, we have analyzed the time courses of product accumulation in these reactions with radioactively labeled substrate. The results, illustrated in Figure 2D, support the conclusions of the fluorescence experiments, showing the opposite-base preference order C > T > G ≈ A. It should be also noted that a highly automatized stopped-flow approach is inherently less prone to sampling irregularities that introduce a large part of the variation during manual sampling in steady-state kinetics. Both visual inspection of the fluorescence curves (Figure 2A) and the calculations of rate constants and their combinations suggest that there are no substantial differences in processing of 8-oxoG·N pairs (N = A, G, or T) by Fpg, at least for the substrates we have used. This preference also coincides with the optimal steric configuration (C > G ≈ T) in the enzyme's active site as determined for Fpg from *B. stearothermophilus* (*27*).

Substrate Specificity of Fpg. The substrates containing mismatched 8-oxoG, or DHU opposite C or G, were different from the 8-oxoG·C substrate in one important respect, evident from Tables 2−4. While all were recognized by Fpg in a five-step process, the efficiency of some steps varied dramatically between 8-oxoG·C, on the one hand, and all other substrates, on the other. The second equilibrium step was especially illustrative, its K_a value being up to 2 orders of magnitude higher for 8-oxoG·C than for other substrates. On the contrary, the third and fourth equilibrium steps were the least efficient for 8-oxoG·C in comparison with the other substrates, especially those containing DHU. These observations indicate that, although Fpg may process a wide range of substrates, there are important differences in the dynamics of these processes. As 8-oxoG·C is considered a physiological substrate for Fpg from a multitude of biochemical and genetic data (reviewed in ref *4*), we regard the kinetic scheme for this lesion as the basic one. In this scheme, the lesion is quickly sequestered into a recognition complex upon encounter, with the following steps being relatively slow; we have recently suggested that this kinetic model would be optimal for minimizing excision errors in a situation of competition with the enzyme sliding off the lesion (*34*). Nonnatural substrates would quickly revert to an encounter complex liable to dissociation; in the case of 8-oxoG·A this would minimize premutagenic excision of 8-oxoG. We conclude that most of the poor substrates studied here are rejected at the first transition energy barrier that the enzyme−substrate complex has to clear on its way to the Michaelis complex. Recently, we have suggested (*20*) that Fpg could encounter the lesion in two different conformations, one associated with the enzyme sliding along DNA, another characteristic of direct binding of the enzyme from solution to the damaged nucleoside, and that the sequence of conformational changes leading to the Michaelis complex might be different in these two cases. Perhaps, the differences in the kinetics of initial stages of enzyme molecule conformational adjustment reflect the existence of these two binding modes, one of which would operate for the correct substrates (such as 8-oxoG·C) and the other, for the nonspecific substrates.

Interestingly, the early rejection of the poor substrates means that they are rejected *before* having a chance to be sampled in the enzyme's active site pocket. Most previous attempts to rationalize Fpg substrate specificity were centered at the specific bonding of the base in the active site (*23*, *28*, *41*, *42*), although an early publication underscored the significance of the pattern of hydrogen bond donors and acceptors presented by 8-oxoG in DNA (*11*). Several computer modeling and experimental studies suggested that physical parameters of DNA, such as its torsional rigidity, resistance to bending, and the base opening rate, may be influenced by the presence of a 8-oxoG residue (*53*−*55*). Thus, we suggest that "indirect readout" using such physicochemical characteristics of the damaged site could be of critical importance for discrimination between correct and incorrect substrates by Fpg. On the other hand, the events in the active site pocket, such as its adjustment to a catalytically competent conformation (characterized by k_5 and k_{-5} in Scheme 2), are of low discriminatory value.

The procedure of substrate discrimination by Fpg is clearly multistage, with many possibilities of rejecting the wrong substrate. Pre-steady-state kinetic analysis of different substrates for this enzyme should clarify the mechanisms operating in the cell to prevent unwelcome excision reactions while allowing efficient repair of oxidatively damaged bases.

ACKNOWLEDGMENT

The authors thank Dr. Dmitri Pyshnyi for the synthesis of substrates.

SUPPORTING INFORMATION AVAILABLE

A derivation of the equations for apparent K_M and k_{cat} using the individual experimentally determined rate constants and the kinetic graph theory and Fpg dynamics during the simulation movie. This material is available free of charge via the Internet at http://pubs.acs.org.

REFERENCES

1. Shibutani, S., Takeshita, M., and Grollman, A. P. (1991) Insertion of specific bases during DNA synthesis past the oxidation-damaged base 8-oxodG, *Nature 349*, 431−434.
2. Kouchakdjian, M., Bodepudi, V., Shibutani, S., Eisenberg, M., Johnson, F., Grollman, A. P., and Patel, D. J. (1991) NMR structural studies of the ionizing radiation adduct 7-hydro-8-oxodeoxyguanosine (8-oxo-7H-dG) opposite deoxyadenosine in

a DNA duplex. 8-Oxo-7H-dG(syn)·dA(anti) alignment at lesion site, *Biochemistry 30*, 1403−1412.
3. McAuley-Hecht, K. E., Leonard, G. A., Gibson, N. J., Thomson, J. B., Watson, W. P., Hunter, W. N., and Brown, T. (1994) Crystal structure of a DNA duplex containing 8-hydroxydeoxyguanine-adenine base pairs, *Biochemistry 33*, 10266−10270.
4. Grollman, A. P., and Moriya, M. (1993) Mutagenesis by 8-oxoguanine: An enemy within, *Trends Genet. 9*, 246−249.
5. Ames, B. N. (1989) Endogenous DNA damage as related to cancer and aging, *Mutat. Res. 214*, 41−46.
6. Ames, B. N., Shigenaga, M. K., and Hagen, T. M. (1993) Oxidants, antioxidants, and the degenerative diseases of aging, *Proc. Natl. Acad. Sci. U.S.A. 90*, 7915−7922.
7. Lu, T., Pan, Y., Kao, S.-Y., Li, C., Kohane, I., Chan, J., and Yankner, B. A. (2004) Gene regulation and DNA damage in the ageing human brain, *Nature 429*, 883−891.
8. Delaney, M. O., Wiederholt, C. J., and Greenberg, M. M. (2002) Fapy·dA induces nucleotide misincorporation translesionally by a DNA polymerase, *Angew. Chem., Int. Ed. 41*, 771−773.
9. Wiederholt, C. J., and Greenberg, M. M. (2002) Fapy·dG instructs Klenow exo$^-$ to misincorporate deoxyadenosine, *J. Am. Chem. Soc. 124*, 7278−7279.
10. Tchou, J., Kasai, H., Shibutani, S., Chung, M.-H., Laval, J., Grollman, A. P., and Nishimura, S. (1991) 8-oxoguanine (8-hydroxyguanine) DNA glycosylase and its substrate specificity, *Proc. Natl. Acad. Sci. U.S.A. 88*, 4690−4694.
11. Tchou, J., Bodepudi, V., Shibutani, S., Antoshechkin, I., Miller, J., Grollman, A. P., and Johnson, F. (1994) Substrate specificity of Fpg protein. Recognition and cleavage of oxidatively damaged DNA, *J. Biol. Chem. 269*, 15318−15324.
12. Michaels, M. L., Cruz, C., Grollman, A. P., and Miller, J. H. (1992) Evidence that MutY and MutM combine to prevent mutations by an oxidatively damaged form of guanine in DNA, *Proc. Natl. Acad. Sci. U.S.A. 89*, 7022−7025.
13. Michaels, M. L., Tchou, J., Grollman, A. P., and Miller, J. H. (1992) A repair system for 8-oxo-7,8-dihydrodeoxyguanine, *Biochemistry 31*, 10964−10968.
14. Bulychev, N. V., Varaprasad, C. V., Dormán, G., Miller, J. H., Eisenberg, M., Grollman, A. P., and Johnson, F. (1996) Substrate specificity of *Escherichia coli* MutY protein, *Biochemistry 35*, 13147−13156.
15. Michaels, M. L., and Miller, J. H. (1992) The GO system protects organisms from the mutagenic effect of the spontaneous lesion 8-hydroxyguanine (7,8-dihydro-8-oxoguanine), *J. Bacteriol. 174*, 6321−6325.
16. Rosenquist, T. A., Zharkov, D. O., and Grollman, A. P. (1997) Cloning and characterization of a mammalian 8-oxoguanine DNA glycosylase, *Proc. Natl. Acad. Sci. U.S.A. 94*, 7429−7434.
17. Fedorova, O. S., Nevinsky, G. A., Koval, V. V., Ishchenko, A. A., Vasilenko, N. L., and Douglas, K. T. (2002) Stopped-flow kinetic studies of the interaction between *Escherichia coli* Fpg protein and DNA substrates, *Biochemistry 41*, 1520−1528.
18. Ishchenko, A. A., Vasilenko, N. L., Sinitsina, O. I., Yamkovoy, V. I., Fedorova, O. S., Douglas, K. T., and Nevinsky, G. A. (2002) Thermodynamic, kinetic, and structural basis for recognition and repair of 8-oxoguanine in DNA by Fpg protein from *Escherichia coli*, *Biochemistry 41*, 7540−7548.
19. Koval, V. V., Kuznetsov, N. A., Zharkov, D. O., Ishchenko, A. A., Douglas, K. T., Nevinsky, G. A., and Fedorova, O. S. (2004) Pre-steady-state kinetics shows differences in processing of various DNA lesions by *Escherichia coli* formamidopyrimidine-DNA glycosylase, *Nucleic Acids Res. 32*, 926−935.
20. Zaika, E. I., Perlow, R. A., Matz, E., Broyde, S., Gilboa, R., Grollman, A. P., and Zharkov, D. O. (2004) Substrate discrimination by formamidopyrimidine-DNA glycosylase: A mutational analysis, *J. Biol. Chem. 279*, 4849−4861.
21. Zharkov, D. O., Shoham, G., and Grollman, A. P. (2003) Structural characterization of the Fpg family of DNA glycosylases, *DNA Repair 2*, 839−862.
22. Karakaya, A., Jaruga, P., Bohr, V. A., Grollman, A. P., and Dizdaroglu, M. (1997) Kinetics of excision of purine lesions from DNA by *Escherichia coli* Fpg protein, *Nucleic Acids Res. 25*, 474−479.
23. Fromme, J. C., and Verdine, G. L. (2003) DNA lesion recognition by the bacterial repair enzyme MutM, *J. Biol. Chem. 278*, 51543−51548.
24. Sugahara, M., Mikawa, T., Kumasaka, T., Yamamoto, M., Kato, R., Fukuyama, K., Inoue, Y., and Kuramitsu, S. (2000) Crystal structure of a repair enzyme of oxidatively damaged DNA, MutM (Fpg), from an extreme thermophile, *Thermus thermophilus* HB8, *EMBO J. 19*, 3857−3869.
25. Gilboa, R., Zharkov, D. O., Golan, G., Fernandes, A. S., Gerchman, S. E., Matz, E., Kycia, J. H., Grollman, A. P., and Shoham, G. (2002) Structure of formamidopyrimidine-DNA glycosylase covalently complexed to DNA, *J. Biol. Chem. 277*, 19811−19816.
26. Serre, L., Pereira de Jésus, K., Boiteux, S., Zelwer, C., and Castaing, B. (2002) Crystal structure of the *Lactococcus lactis* formamidopyrimidine-DNA glycosylase bound to an abasic site analogue-containing DNA, *EMBO J. 21*, 2854−2865.
27. Fromme, J. C., and Verdine, G. L. (2002) Structural insights into lesion recognition and repair by the bacterial 8-oxoguanine DNA glycosylase MutM, *Nat. Struct. Biol. 9*, 544−552.
28. Coste, F., Ober, M., Carell, T., Boiteux, S., Zelwer, C., and Castaing, B. (2004) Structural basis for the recognition of the FapydG lesion (2,6-diamino-4-hydroxy-5-formamidopyrimidine) by formamidopyrimidine-DNA glycosylase, *J. Biol. Chem. 279*, 44074−44083.
29. Buchko, G. W., McAteer, K., Wallace, S. S., and Kennedy, M. A. (2005) Solution-state NMR investigation of DNA binding interactions in *Escherichia coli* formamidopyrimidine-DNA glycosylase (Fpg): A dynamic description of the DNA/protein interface, *DNA Repair 4*, 327−339.
30. Johnson, K. A., Ed. (2003) *Kinetic Analysis of Macromolecules*, Oxford University Press, Oxford.
31. Fisher, H. F. (2005) Transient-state kinetic approach to mechanisms of enzymatic catalysis, *Acc. Chem. Res. 38*, 157−166.
32. Porello, S. L., Leyes, A. E., and David, S. S. (1998) Single-turnover and pre-steady-state kinetics of the reaction of the adenine glycosylase MutY with mismatch-containing DNA substrates, *Biochemistry 37*, 14756−14764.
33. Bernards, A. S., Miller, J. K., Bao, K. K., and Wong, I. (2002) Flipping duplex DNA inside out: a double base-flipping reaction mechanism by *Escherichia coli* MutY adenine glycosylase, *J. Biol. Chem. 277*, 20960−20964.
34. Zharkov, D. O., and Grollman, A. P. (2005) The DNA trackwalkers: Principles of lesion search and recognition by DNA glycosylases, *Mutat. Res. 577*, 24−54.
35. Kuzmic, P. (1996) Program DYNAFIT for the analysis of enzyme kinetic data: application to HIV proteinase, *Anal. Biochem. 237*, 260−273.
36. Vorobjev, Y. N. (2005) Study of the mechanism of interaction of oligonucleotides with the 3′-terminal region of tRNA^{Phe} by computer modeling, *Mol. Biol.* (*Moscow*) *39*, 777−784.
37. Cornell, W. D., Cieplak, P., Bayly, C. I., Gould, I. R., Merz, K. M., Ferguson, D. M., Spellmeyer, D. C., Fox, T., Caldwell, J. W., and Kollman, P. A. (1995) A second generation force field for the simulation of proteins, nucleic acids, and organic molecules, *J. Am. Chem. Soc. 117*, 5179−5197.
38. Gallicchio, E., and Levy, R. M. (2004) AGBNP: an analytic implicit solvent model suitable for molecular dynamics simulations and high-resolution modeling, *J. Comput. Chem. 25*, 479−499.
39. Lakowicz, J. R., Ed. (1999) *Principles of Fluorescence Spectroscopy*, 2nd ed., Kluwer Academic/Plenum Publishers, New York.
40. Amadei, A., Linssen, A. B., and Berendsen, H. J. (1993) Essential dynamics of proteins, *Proteins 17*, 412−425.
41. Amara, P., Serre, L., Castaing, B., and Thomas, A. (2004) Insights into the DNA repair process by the formamidopyrimidine-DNA glycosylase investigated by molecular dynamics, *Protein Sci. 13*, 2009−2021.
42. Perlow-Poehnelt, R. A., Zharkov, D. O., Grollman, A. P., and Broyde, S. (2004) Substrate discrimination by formamidopyrimidine-DNA glycosylase: Distinguishing interactions within the active site, *Biochemistry 43*, 16092−16105.
43. Wong, I., Lundquist, A. J., Bernards, A. S., and Mosbaugh, D. W. (2002) Presteady-state analysis of a single catalytic turnover by *Escherichia coli* uracil-DNA glycosylase reveals a "pinch-pull-push" mechanism, *J. Biol. Chem. 277*, 19424−19432.
44. Jiang, Y. L., Kwon, K., and Stivers, J. T. (2001) Turning on uracil-DNA glycosylase using a pyrene nucleotide switch, *J. Biol. Chem. 276*, 42347−42354.
45. Jiang, Y. L., and Stivers, J. T. (2002) Mutational analysis of the base-flipping mechanism of uracil DNA glycosylase, *Biochemistry 41*, 11236−11247.
46. Jiang, Y. L., Stivers, J. T., and Song, F. (2002) Base-flipping mutations of uracil DNA glycosylase: Substrate rescue using a pyrene nucleotide wedge, *Biochemistry 41*, 11248−11254.
47. Slupphaug, G., Mol, C. D., Kavli, B., Arvai, A. S., Krokan, H. E., and Tainer, J. A. (1996) A nucleotide-flipping mechanism from

the structure of human uracil-DNA glycosylase bound to DNA, *Nature 384*, 87−92.
48. Bjørås, M., Seeberg, E., Luna, L., Pearl, L. H., and Barrett, T. E. (2002) Reciprocal "flipping" underlies substrate recognition and catalytic activation by the human 8-oxo-guanine DNA glycosylase, *J. Mol. Biol. 317*, 171−177.
49. Golan, G., Zharkov, D. O., Feinberg, H., Fernandes, A. S., Zaika, E. I., Kycia, J. H., Grollman, A. P., and Shoham, G. (2005) Structure of the uncomplexed DNA repair enzyme endonuclease VIII indicates significant interdomain flexibility, *Nucleic Acids Res. 33*, 5006−5016.
50. Castaing, B., Geiger, A., Seliger, H., Nehls, P., Laval, J., Zelwer, C., and Boiteux, S. (1993) Cleavage and binding of a DNA fragment containing a single 8-oxoguanine by wild type and mutant FPG proteins, *Nucleic Acids Res. 21*, 2899−2905.
51. Asagoshi, K., Yamada, T., Terato, H., Ohyama, Y., Monden, Y., Arai, T., Nishimura, S., Aburatani, H., Lindahl, T., and Ide, H. (2000) Distinct repair activities of human 7,8-dihydro-8-oxoguanine DNA glycosylase and formamidopyrimidine DNA glycosylase for formamidopyrimidine and 7,8-dihydro-8-oxoguanine, *J. Biol. Chem. 275*, 4956−4964.
52. Plum, G. E., Grollman, A. P., Johnson, F., and Breslauer, K. J. (1995) Influence of the oxidatively damaged adduct 8-oxodeoxyguanosine on the conformation, energetics, and thermodynamic stability of a DNA duplex, *Biochemistry 34*, 16148−16160.
53. Pinak, M. (2003) Electrostatic energy analysis of 8-oxoguanine DNA lesion—molecular dynamics study, *Comput. Biol. Chem. 27*, 431−441.
54. Barone, F., Dogliotti, E., Cellai, L., Giordano, C., Bjørås, M., and Mazzei, F. (2003) Influence of DNA torsional rigidity on excision of 7,8-dihydro-8-oxo-2′-deoxyguanosine in the presence of opposing abasic sites by human OGG1 protein, *Nucleic Acids Res. 31*, 1897−1903.
55. Miller, J. H., Fan-Chiang, C.-C. P., Straatsma, T. P., and Kennedy, M. A. (2003) 8-Oxoguanine enhances bending of DNA that favors binding to glycosylases, *J. Am. Chem. Soc. 125*, 6331−6336.
56. Huang, C. Y. (1979) Derivation of initial velocity and isotope exchange rate equations, *Methods Enzymol. 63*, 54−84.

BI060787R